Low-lying electric and magnetic dipole strengths in ^{207}Pb

T. Shizuma,[1] F. Minato,[2] M. Omer,[3,*] T. Hayakawa,[1,4] H. Ohgaki,[5] and S. Miyamoto[6]

[1]*National Institutes for Quantum and Radiological Science and Technology, Tokai, Ibaraki 319-1106, Japan*

[2]*Nuclear Data Center, Japan Atomic Energy Agency, Tokai, Ibaraki 319-1195, Japan*

[3]*Integrated Support Center for Nuclear Nonproliferation and Nuclear Security, Japan Atomic Energy Agency, Tokai, Ibaraki 319-1195, Japan*

[4]*Institute of Laser Engineering, Osaka University, Suita, Osaka 565-0871 Japan*

[5]*Institute of Advanced Energy, Kyoto University, Uji, Kyoto 611-0011, Japan*

[6]*Laboratory of Advanced Science and Technology for Industry, University of Hyogo, Kamigori, Hyogo 678-1205, Japan*

(Received 25 September 2020; accepted 22 January 2021; published 5 February 2021)

Low-lying dipole transitions in ^{207}Pb were measured via nuclear photon scattering using a quasimonochromatic, linearly polarized photon beam. The spins and/or parities of the states observed in ^{207}Pb were determined from the intensity asymmetry of resonantly scattered γ rays with respect to the polarization plane of the incident photon beam. The electric ($E1$) and magnetic ($M1$) dipole strengths were obtained for excitation energies from 5.49 to 6.75 MeV. The present experimental results, combined with (γ, n) data from the literature, were used to investigate the $E1$ and $M1$ photoabsorption cross sections near the neutron separation energy by comparison with predictions from the particle-vibration coupling with the quasiparticle random-phase approximation model.

DOI: 10.1103/PhysRevC.103.024309

I. INTRODUCTION

The low-lying electric ($E1$) and magnetic ($M1$) dipole excitations in atomic nuclei have attracted interest during the past decades [1,2]. The observation of such excitations provides valuable information on collective and single-particle motions. Nuclei close to the doubly closed-shell nucleus ^{208}Pb are suitable for investigating the spin-flip $M1$ mode [3]. In the independent-particle model, the $M1$ excitation to the lowest two 1^+ states in ^{208}Pb is expected to be the 1 particle, 1 hole (1p-1h) spin-flip excitation of $\pi(1h^{-1}_{11/2}, 1h^{1}_{9/2})$ and $\nu(1i^{-1}_{13/2}, 1i^{1}_{11/2})$. The mixing of these unperturbed states by the residual proton-neutron interaction causes isoscalar (IS) and isovector (IV) states. Experimentally, the IS and IV 1^+ states in ^{208}Pb have been observed at 5.85 MeV and approximately 7.1–8.7 MeV, respectively [4–6]. Since the nucleus ^{207}Pb differs from ^{208}Pb by one less neutron, such $M1$ resonances could be present. In a previous $(\vec{\gamma}, n)$ measurement [7], an $M1$ strength concentration was observed just above the neutron separation energy ($S_n = 6.737$ MeV) in ^{207}Pb. However, detailed information on the $M1$ strength below this energy is scarce.

The local accumulation of $E1$ strength near the particle threshold has been observed in both stable and unstable nuclei over a broad range of nuclei [8–17]. This phenomenon is commonly referred to as the pygmy dipole resonance (PDR) because the measured $E1$ strength is weak relative to that of the giant dipole resonance (GDR), which is the main part of the $E1$ strength in nuclei. The PDR may provide useful information on fundamental nuclear properties such as the neutron-skin thickness and the symmetry energy parameter in the nuclear equation of state at densities relevant to neutron stars [18,19]. The total sum of the measured energy-weighted $E1$ strength of the PDR is less than approximately 1% of the Thomas-Reiche-Kuhn (TRK) sum rule value for stable nuclei and approximately 5% of that for unstable neutron-rich nuclei. For stable lead isotopes, the values of 0.300(52)% and 0.705(52)% were observed for ^{206}Pb and ^{208}Pb [20], respectively, below the excitation energy of $E = 6.75$ MeV.

Previously, the low-lying dipole strength distribution in ^{207}Pb was studied by using nuclear resonance fluorescence (NRF) [21–26]. While the spins and parities of the states at 5490, 5598, and 5611 keV are known from previous work [26], those of the higher-lying states remain to be revealed. In this paper, we report the results of a NRF measurement of ^{207}Pb using a quasimonochromatic, linearly polarized photon beam generated by laser Compton scattering (LCS). The experimental results are compared with predictions from the particle-vibration coupling [27] with the quasiparticle random-phase approximation model [28] (PVC + QRPA) using Skyrme effective forces.

II. EXPERIMENTAL PROCEDURE

The present NRF experiment was performed at the Laboratory of Advanced Science and Technology for Industry (LASTI) at the University of Hyogo. A quasimonochromatic, linearly polarized photon beam was generated by LCS with relativistic electrons circulating in the NewSUBARU storage ring [29,30]. A Nd:YVO_4 laser with a 1064-nm wavelength operated at a 20-kHz frequency was used. The electron energies of 571, 595, and 620 MeV were selected to produce LCS photons with maximum energies $E_\gamma^{\max}$ of 5.8, 6.3, and 6.8 MeV, respectively. A lead collimator with a

*Present address: Physics Department, Faculty of Science, Assiut University, Assiut 71516, Egypt.

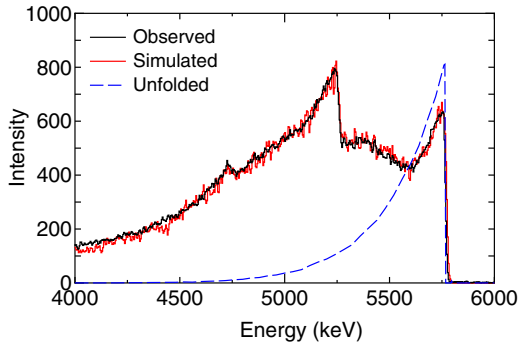

FIG. 1. Typical energy distribution of the incident photon beam with $E_\gamma^{\max} = 5.8$ MeV measured using the HPGe detector (black line). The original LCS photon spectrum (blue dashed line) was obtained by unfolding the simulated energy distribution (red line).

10-cm thickness and a 4-mm aperture was used to form a quasimonochromatic photon beam with an energy spread of $\Delta E/E \approx 4\%$ at full width at half maximum (FWHM). The photon flux was measured during the NRF measurement at each LCS photon energy by a large volume ($8'' \times 12''$) NaI(Tl) scintillation detector. The average intensity on the target was 4×10^5 photons per second. The target consisted of a metallic cylinder (8 mm in diameter) of ^{207}Pb (13.9 g) enriched to 98.1%. In addition, a ^{208}Pb target (6.2 g, enriched to 98.4%) was used for strength normalization of NRF γ rays.

Two high-purity germanium (HPGe) detectors with efficiencies of 120% and 140% relative to a $3'' \times 3''$ NaI scintillation detector were used to measure photons scattered from the target. These detectors were fixed in the horizontal plane at a scattering angle of $\theta = 90^\circ$. The polarization of the LCS photon beam was varied into the vertical and horizontal planes to determine the spins and parities of the excited states discussed later. The typical energy resolution of the HPGe detectors was $\Delta E_\gamma/E_\gamma \approx 0.09\%$ at $E_\gamma \approx 7$ MeV. The γ-ray energies were calibrated using a natural background γ ray (2614.5 keV) and the known $E1$ peaks at 7063 and 7083 keV in ^{208}Pb. In addition, we calculated the relative efficiencies for the HPGe detectors using Electron Gamma Shower (EGS5) [31]. The calculated efficiency curves were verified using efficiencies obtained from measurements with a ^{152}Eu standard source and the known resonances in ^{208}Pb.

Figure 1 shows a typical energy spectrum for an incident photon beam with $E_\gamma^{\max} = 5.8$ measured by the HPGe detector. A Monte Carlo simulation was performed with the EGS5 code to analyze the HPGe detector response. The energy distribution of the incident photon beam was extracted by unfolding the simulated spectrum to reproduce the observed energy distribution, as shown in Fig. 1.

III. RESULTS

Figure 2 presents parts of the photon-scattering spectra observed at a polar angle of $\theta = 90^\circ$ relative to the incident photon beam with $E_\gamma^{\max} = 5.8$, 6.3, and 6.8 MeV. These spectra were obtained at azimuthal angles of $\phi = 0^\circ$ and 90° relative to the polarization plane formed by the propagation

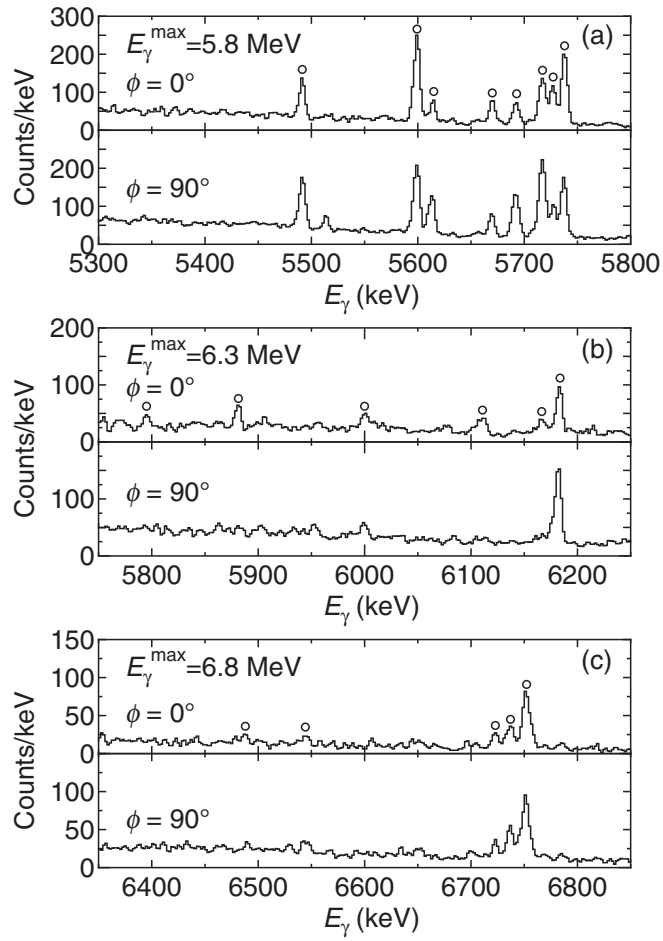

FIG. 2. Photon-scattering spectra observed at a polar angle of $\theta = 90^\circ$ relative to the incident photon beam and azimuthal angles of $\phi = 0^\circ$ (top) and 90° (bottom) relative to the polarization plane of the LCS photon beam with (a) $E_\gamma^{\max} = 5.8$, (b) 6.3, and (c) 6.8 MeV. The transitions to the ground state in ^{207}Pb are labeled with open circles in the upper panels.

direction of the electric-field vector of the incident photon beam.

Considering dipole excitations of the $J_0^\pi = 1/2^-$ ground state of ^{207}Pb, the spins and parities of the excited states could only be $J^\pi = 1/2^\pm, 3/2^\pm$. The intensity distribution function of a $1/2^- \to 3/2^\pm \to 1/2^-$ photon-scattering cascade using a polarized photon beam is given by

$$W(\theta, \phi) = W(\theta) \mp \tfrac{3}{8}(1 - \cos^2\theta)\cos 2\phi, \qquad (1)$$

where $W(\theta)$ is the angular-correlation function for an unpolarized photon beam, expressed as $\frac{3}{8}\cos^2\theta + \frac{7}{8}$. A more general form of Eq. (1) can be found in Ref. [32].

To determine the spins and parities of the observed states, we used the azimuthal intensity ratio defined by

$$R = \frac{W(90^\circ, 90^\circ)}{W(90^\circ, 0^\circ)}. \qquad (2)$$

Under the condition of complete polarization of the incoming photon beam, R is expected to be 0.4 for $J^\pi = 3/2^-$ and 2.5

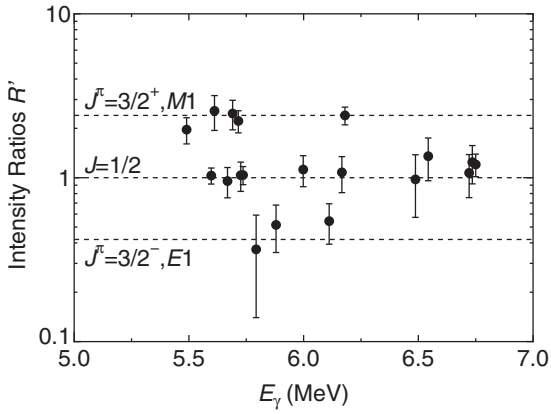

FIG. 3. Measured azimuthal intensity ratios R' for the dipole transitions of ^{207}Pb. The horizontal lines $R' = 0.42$, 1, and 0.24 indicate the calculated ratios for $J^\pi = 3/2^-$, $J^\pi = 1/2^\pm$, and $J^\pi = 3/2^+$, respectively.

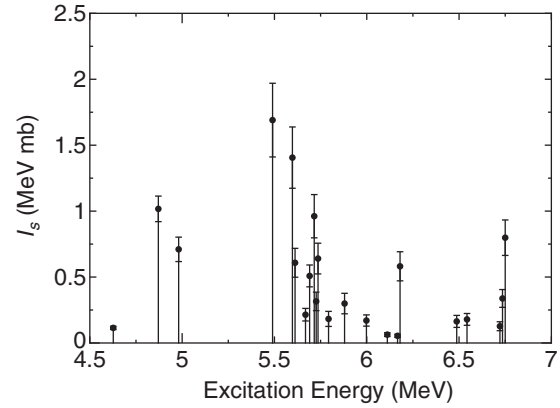

FIG. 4. Integrated scattering cross sections deduced from the present experiment. Data below 5 MeV are taken from Ref. [35].

for $J^\pi = 3/2^+$. However, these ratios slightly deviate from the ideal values because of the finite solid angle of the HPGe detectors and the spatially extended target. For the present case, the ratios are deduced from the numerical simulation to be 0.42 for $J^\pi = 3/2^-$ and 2.4 for $J^\pi = 3/2^+$. For a $1/2^- \rightarrow 1/2^\pm \rightarrow 1/2^-$ photon-scattering cascade, an excited $J = 1/2$ state radiates isotropically, and hence, R equals unity for $J = 1/2^\pm$.

The corresponding measured intensity ratios are given by $R' = N_\perp/N_\parallel$ where $N_\perp$ ($N_\parallel$) represents the intensity of resonant photons detected in the plane perpendicular (parallel) to the polarization plane at $\theta = 90^\circ$. From the comparison between measured and calculated azimuthal intensity ratios, the spins and/or parities of the excited states were determined as presented in Fig. 3.

In photon-scattering measurements, the energy-integrated scattering cross section I_s of a state at the excitation energy E_x can be deduced from the measured intensities of the respective transitions to the ground state [33]. In the present study, this cross section was determined relative to the known integrated scattering cross section $I_s(E_x^{\mathrm{Ref}})$ of the state at 7332 keV in ^{208}Pb:

$$\frac{I_s(E_x)}{I_s\left(E_x^{\mathrm{Ref}}\right)} = \left[\frac{I_\gamma(E_\gamma)}{W(\theta;E_\gamma)\Phi_\gamma(E_x)N_N\lambda(E_x)}\right] \times \left[\frac{I_\gamma\left(E_\gamma^{\mathrm{Ref}}\right)}{W\left(\theta;E_\gamma^{\mathrm{Ref}}\right)\Phi_\gamma\left(E_x^{\mathrm{Ref}}\right)N_N^{\mathrm{Ref}}\lambda\left(E_x^{\mathrm{Ref}}\right)}\right]^{-1}.$$

Here, $I_\gamma(E_\gamma)$ and $I_\gamma(E_\gamma^{\mathrm{Ref}})$ denote the efficiency-corrected intensities of a ground-state transition at E_γ in ^{207}Pb and of the 7332-keV transition in ^{208}Pb, respectively, obtained using summed spectra of γ rays emitted parallel and perpendicular to the polarization plane. $W(\theta;E_\gamma)$ and $W(\theta;E_\gamma^{\mathrm{Ref}})$ are the angular distribution functions for these transitions at $\theta = 90^\circ$ for an unpolarized photon beam. The quantities $\Phi(E_x)$ and $\Phi_\gamma(E_x^{\mathrm{Ref}})$ are the photon fluxes at the energy of the considered level and at the energy of ^{208}Pb, respectively. The quantities N_N and N_N^{Ref} represent the numbers of nuclei in the ^{207}Pb and ^{208}Pb targets, respectively. The quantities $\lambda(E_x)$ and $\lambda(E_x^{\mathrm{Ref}})$ are the correction factors of the atomic and nuclear self-absorption for the levels at E_x in ^{207}Pb and E_x^{Ref} in ^{208}Pb. These correction factors were determined according to Eq. (19) in Ref. [34]. The present determination of the integrated cross sections relative to the state in ^{208}Pb has the advantage that the efficiencies of the detectors and the photon flux are needed in relative units only.

The integrated scattering cross section I_s is related to the total decay width Γ and the partial decay width Γ_0 to the ground state according to

$$I_s = \left(\frac{\pi\hbar c}{E_x}\right)^2 \frac{g\Gamma_0^2}{\Gamma}, \tag{3}$$

where g is a spin factor defined as $(2J_x + 1)/(2J_0 + 1)$ with J_0 and J_x being the spins of the ground state and the excited state, respectively.

The experimental results are summarized in Table I. We observed 19 dipole states at excitation energies between 5.49 and 6.75 MeV, of which seven states (marked with the superscript "a" in Table I) were newly found. The spins and/or parities of 15 states were newly assigned based on the azimuthal intensity ratios. The assignments of $J^\pi = 3/2^+$ for the 5.490 and 5.612-MeV states and $J = 1/2$ for the 5.598-MeV state are consistent with the results presented in Ref. [26]. The assignment of $J^\pi = 3/2^+$ for the 5690.6-keV level is also consistent with $(3/2^+)$ in Ref. [35]. A comparison of the $g\Gamma_0^2/\Gamma$ ratios obtained in the present experiment with those from previous work [22,23,25] is also shown in Table I. The present results are generally in good agreement with those previously reported.

IV. DISCUSSION

The integrated scattering cross sections deduced from the present NRF experiments are shown in Fig. 4. The large strengths below 6.8 MeV are carried by two ground-state transitions from the 5.490 and 5.612-MeV states. While these states are considered to predominately originate in the weak coupling of the $\nu 3p_{1/2}^{-1}$ neutron hole to the ^{208}Pb $J^\pi = 1^-$ core at 5.512 MeV, the corresponding strengths are three times

TABLE I. Excitation energies E_x, spins and parities J^π, ratios $g\Gamma_0^2/\Gamma$, branching ratios to the ground state Γ_0/Γ, and reduced transition probabilities $B(E1)\uparrow$ and $B(M1)\uparrow$ obtained in the present work. The $g\Gamma_0^2/\Gamma$ values reported in previous work are listed for comparison.

E_x (keV)	J^π[a]	J^π (lit.)	$g\Gamma_0^2/\Gamma$[a] (eV)	Γ_0/Γ	$B(E1)\uparrow$ $\times 10^{-3}$ (e^2 fm^2)	$B(M1)\uparrow$ (μ_N^2)	$g\Gamma_0^2/\Gamma$[b] (eV)	$g\Gamma_0^2/\Gamma$[c] (eV)	$g\Gamma_0^2/\Gamma$[d] (eV)
5490.0(3)	$3/2^+$	$3/2^+$[e]	13.3(22)	1.0[f]	77(13)		11.57(139)	11.4(19)	12
5597.5(3)	$1/2$	$1/2$[e]	11.5(19)	1.0	63(10)	5.7(9)	12.09(141)	9.0(14)	8
5611.6(4)	$3/2^+$	$3/2^+$[e]	5.0(9)	1.0	27(5)			5.5(9)	
5668.3(4)[g]	$1/2$		1.8(4)	1.0	9.4(21)	0.87(17)			
5690.6(4)	$3/2^+$	$(3/2^+)$[h]	4.3(7)	0.78(7)[i]	29(6)		1.97(135)	3.0(6)	
5715.6(3)	$3/2^+$	$1/2, 3/2$[b]	8.2(14)	1.0	42(7)		7.77(112)	6.2(12)	3
5726.0(4)[a]	$1/2$		2.7(6)	0.72(7)[j]	19(5)	1.7(4)			
5736.1(3)	$1/2$		5.5(10)	0.74(5)[j]	38(7)	3.4(6)		5.1(11)	
5793.1(9)	$3/2^-$		1.6(5)	1.0		0.71(22)		2.4(10)	
5879.8(6)[a]	$3/2^-$		2.7(7)	1.0		1.1(3)			
5998.3(6)[a]	$1/2$		1.6(4)	1.0	7.1(18)	0.64(16)			
6111.4(7)[a]	$3/2^-$		0.62(14)	1.0		0.23(5)			
6166.8(7)[a]	$1/2$		0.54(12)	1.0	2.2(5)	0.20(4)			
6180.3(3)	$3/2^+$	$1/2, 3/2$[b]	5.8(11)	0.70(6)[j]	34(7)		5.93(119)	3.3(7)	
6487.4(7)[a]	$1/2$		1.8(5)	1.0	6.3(17)	0.56(15)			
6543.1(7)	$1/2$		2.0(5)	1.0	6.8(17)	0.62(14)		2.3(6)	
6721.5(5)[a]	$1/2$		1.5(4)	1.0	4.7(13)	0.43(11)			
6735.3(5)	$1/2$		4.0(8)	1.0	12.5(25)	1.13(22)		2.7(7)	
6750.1(4)	$1/2$		9.5(16)	1.0	29(5)	2.7(5)		7.2(14)	<10

[a]This work.
[b]Taken from Ref. [25].
[c]Taken from Ref. [23].
[d]Taken from Ref. [22]. Uncertainty in excess of 50% quoted.
[e]Taken from Ref. [26].
[f]Possible decay branch to the first excited state was reported in previous work [25]. However, such a branching transition was not observed in the present experiment.
[g]The level likely corresponds to the 5668-keV level reported in Ref. [36].
[h]Taken from Ref. [35].
[i]Decay branch to the first excited state was observed in the present NRF experiment.
[g]Decay branch to the second excited state was observed in the present NRF experiment.

smaller than that of the ^{208}Pb core, indicating a substantial deviation from the pure weak-coupling picture due to the particle-core coupling [26].

The reduced transition probabilities $B(E1)\uparrow$ and $B(M1)\uparrow$ can be extracted from $g\Gamma_0$ using the following relationships:

$$B(E1)\uparrow = 0.955\frac{g\Gamma_0}{E_\gamma^3}\ [10^{-3}\ e^2\ \mathrm{fm}^2], \tag{4}$$

$$B(M1)\uparrow = 0.0866\frac{g\Gamma_0}{E_\gamma^3}\ [\mu_N^2], \tag{5}$$

where Γ_0 is given in units of meV and E_γ in units of MeV.

The deduced $E1$ and $M1$ transition probabilities are listed in Table I. From the present work, the total $E1$ strength of $\Sigma B(E1) = 0.407(23)\ e^2$ fm^2 at excitation energies from 5 to 6.8 MeV was obtained assuming an $E1$ nature for the transitions from the $J = 1/2$ states. If one assumes $M1$ strengths for the transitions from the $J = 1/2$ states in ^{207}Pb comparable to those in ^{206}Pb [17] and ^{208}Pb [6], then our results on the total $E1$ strength would change by at most 10%. Therefore, this assumption does not affect the conclusions on the gross properties of the $E1$ strength distribution discussed below. The total $E1$ strength below 5 MeV is known to be $\Sigma B(E1) = 0.043(5)\ e^2$ fm^2 from previous (γ, γ') measurements [21,23–25]. By adding this value to the present result, the total $E1$ strength below 6.8 MeV is $\Sigma B(E1) = 0.45(2)\ e^2$ fm^2. This value corresponds to 0.35(2)% of the energy-weighted TRK sum-rule value, which is comparable to the value of 0.300(52)% for ^{206}Pb and one-half the value of 0.705(52)% for ^{208}Pb [20].

Three $M1$ transitions to the ground state from the $J^\pi = 3/2^-$ states at 5.793, 5.880, and 6.111 MeV were observed with a total $M1$ strength of $\Sigma B(M1) = 2.1(4)\mu_N^2$. This value is comparable to the $M1$ strength of $2.0(3)\mu_N^2$ [6] for the transition at 5.844 MeV in ^{208}Pb, which is usually referred to as an IS spin-flip $M1$ mode with in-phase proton and neutron motion [3,37]. At higher energy ($7 < E_x < 7.35$ MeV), a larger $M1$ strength, $\Sigma B(M1) = 9.2(14)\mu_N^2$, is known for ^{208}Pb [6], which is caused by an IV spin-flip $M1$ mode with out-of-phase proton-neutron motion. The neutron separation energy of ^{207}Pb is, however, lower than the excitation energy for this $M1$ mode, so the photon-scattering experiment is not sensitive to the observation of an IV $M1$ excitation.

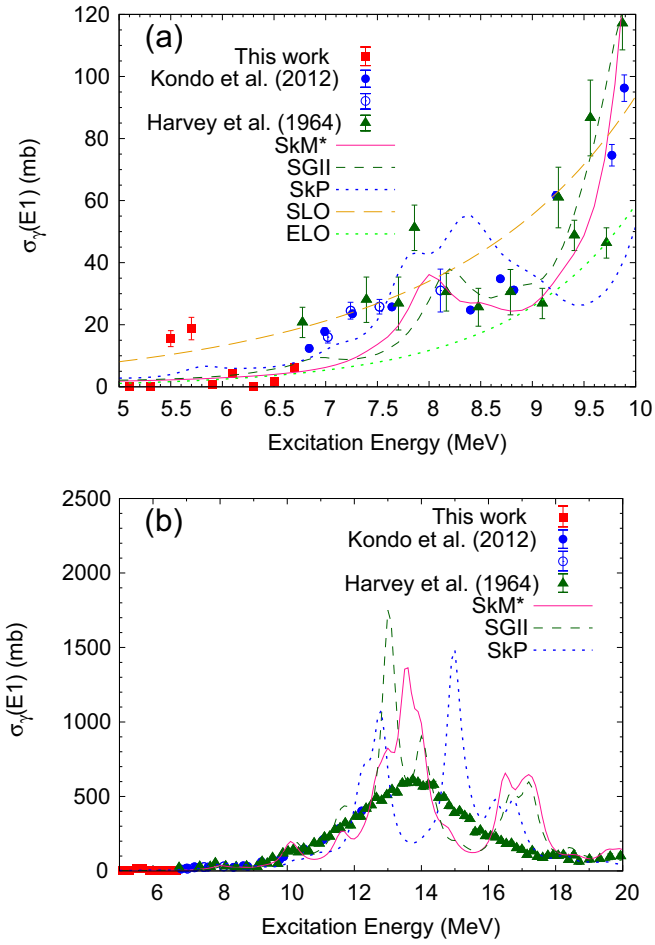

FIG. 5. $E1$ photoabsorption cross sections in the energy range (a) from 5 to 10 MeV and (b) from 5 to 20 MeV, obtained from the present $(\vec{\gamma}, \gamma')$ experiment (red squares) and from $(\vec{\gamma}, n)$ [7] (blue open circles) and (γ, n) [7,38] (blue filled circles and green triangles) experiments compared with the PVC + QRPA calculations using the SkM* (red line), SGII (green broken line), and SkP (blue dotted line) forces. Also shown are the Lorentzian curves with constant width (long broken line) and an energy-dependent width (green dotted line) from RIPL3 [42].

The photoabsorption cross section σ_γ can be obtained from $g\Gamma_0$ by the following equation:

$$\int \sigma_\gamma dE = (\pi\hbar c)^2 \Sigma \frac{g\Gamma_0}{E_\gamma^2}. \quad (6)$$

The $E1$ photoabsorption cross sections (binned in 200 keV steps) deduced from the present $(\vec{\gamma}, \gamma')$ experiment are shown with those obtained from $(\vec{\gamma}, n)$ or (γ, n) experiments [7,38] in Figs. 5(a) and 5(b). Note that the data from Ref. [38] are scaled up by a factor of 1.22 according to the suggestion in Ref. [39]. Comparing the measured $E1$ photoabsorption cross sections with an extrapolation of the GDR is interesting to judge whether the low-lying strength is simply a part of the GDR. In Fig. 5(a), two Lorentzian curves show an extrapolation of the GDR assuming a constant width (SLO) and an energy-dependent width (ELO). From neutron capture reactions and measurements of γ-ray strength functions close to the particle threshold, it is known that the extrapolation of the Lorentzian curve with the constant width overestimates the $E1$ strength in nuclei around closed shells. Hence, the use of the Lorentzian with the energy-dependent width was suggested [40,41]. From the systematic analysis using the quasiparticle phonon model (QPM), the $E1$ strengths observed in ^{204,206,208}Pb below 6.5 MeV were concluded to not be attributable to an oscillation of the excess neutrons with respect to the remaining core [41]. The low-lying $E1$ strength found in ^{207}Pb is consistent with this picture. In contrast, an $E1$ strength concentration (corresponding to 0.32% of the energy-weighted TRK sum rule value) approximately 7.5 MeV above the neutron separation energy of ^{207}Pb was found in the $(\vec{\gamma}, n)$ experiment, indicating the presence of a PDR [7].

The measured $E1$ photoabsorption cross sections are also compared with the PVC + QRPA calculations [27] based on the nonrelativistic Skyrme energy density functional (EDF) [43–45]. To calculate the excited states of ^{207}Pb, core-polarization effects were treated using a PVC model [46,47]. We assumed ^{207}Pb as a two-body system consisting of the ^{206}Pb core nucleus and one neutron. Then, we considered the coupling between the core nucleus states and one-neutron quasiparticle states when calculating the excited states of ^{207}Pb. We introduced two modifications from Refs. [46,47]: (i) The core nucleus of ^{206}Pb and neutron quasiparticle states were computed by the self-consistent Hartree-Fock + BCS model with Skyrme effective forces (SHF-BCS) [43,44], and to calculate the excited states of ^{206}Pb, the QRPA on the basis of SHF-BCS was used: (ii) In the BCS approximation, blocking effects [28] were introduced for the $2p_{1/2}$ neutron state that was supposed to be occupied by the last neutron of ^{207}Pb.

Variations arising from Skyrme effective forces were checked by using three different parameter sets, SkM* [48], SGII [49], and SkP [50]. The calculated $E1$ resonances were folded by the Lorentzian function with a width of $\Gamma_{E1} =$ 0.5 MeV. The predicted photoabsorption cross sections in the energy region from 5 to 10 MeV are shown in Fig. 5(a). The PVC + QRPA calculations are in reasonable agreement with the experimental data above ≈6 MeV. A small bump observed around 8 MeV is reproduced for all three Skyrme forces. In this energy region, the amplitude of the neutron oscillation of the $E1$ resonances is much larger than that of the proton oscillation at the nuclear surface (≈8 fm). This is consistent with the interpretation of the presence of a PDR in ^{207}Pb noted by Kondo *et al.* [7].

The calculated photoabsorption cross sections do not agree with the experimental data around $E = 5.5$ MeV as shown in Fig. 5(a). Although several resonances are predicted by the PVC + QRPA calculations in this energy region, they are smeared by the relatively large contribution from resonances at high energies. We therefore depict the predicted $E1$ strength in a discrete style in Fig. 6. The calculation with the SkP force shows some resonances around $E = 5.5$ MeV. Although the calculations with the SkM* and SGII forces show resonances at higher energy than SkP ($E = 6.5$–7.5 MeV), these resonances are never reproduced without the coupling of the particle with the core. The main configurations of

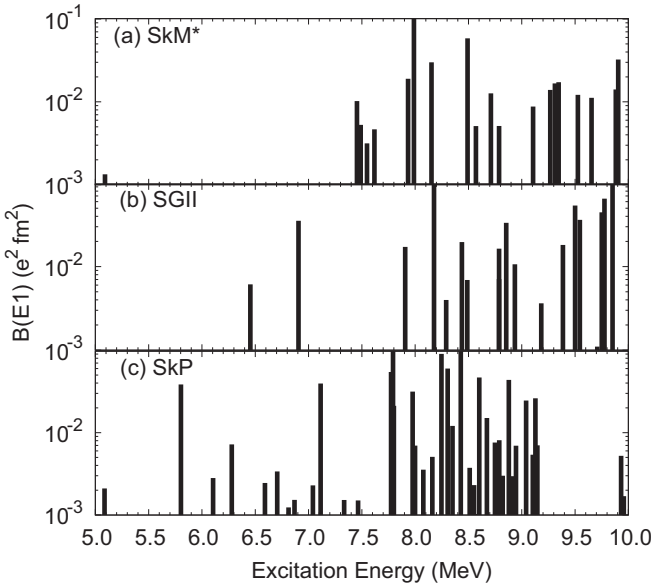

FIG. 6. $E1$ strength predicted by the PVC + QRPA calculation using the (a) SkM*, (b) SGII, and (c) SkP forces.

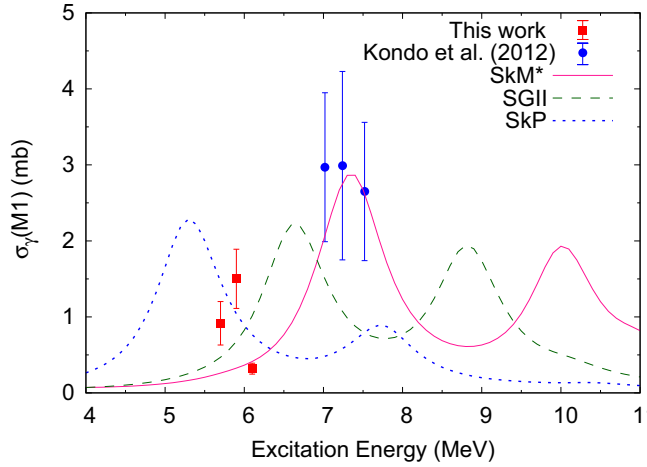

FIG. 7. $M1$ photoabsorption cross sections obtained from the present $(\vec{\gamma}, \gamma')$ experiment (red squares) and from the $(\vec{\gamma}, n)$ experiment (blue circles) [7] compared with the PVC + QRPA calculation using the SkM* (red line), SGII (green broken line), and SkP (blue dotted line) forces.

the resonant states are $\nu p_{3/2} \otimes 3^-_{1,2}$ and $\nu f_{5/2} \otimes 3^-_2$ for the SkP force, $\nu p_{3/2} \otimes 3^-_2$ and $\nu f_{5/2} \otimes 3^-_1$ for the SkM* force, and $\nu f_{5/2} \otimes 3^-_{1,2}$ and $\nu s_{1/2} \otimes 0^+_1$ for the SGII force. Here, 0^+_1, 3^-_1, and 3^-_2 represent the ground state, the first 3^- state, and the second 3^- state, respectively, in the ^{206}Pb core. The importance of the coupling with the low-lying 3^- states of the core nucleus is known from previous work [51] where excited levels of ^{209}Pb and ^{209}Bi were described by the PVC model considering ^{208}Pb as a core nucleus. The $E1$ photoabsorption cross section from 5 to 20 MeV including the GDR region is shown in Fig. 5(b). The PVC + QRPA calculations give a higher peak with a narrower width than the experimental data. This is because the present QRPA framework considers only up to 1p-1h excitation of the ^{206}Pb core. Collisional damping, i.e., a spreading width, is not properly generated. This is one of the general aspects of QRPA calculations. To avoid this shortcoming, a large Lorentzian width (e.g., $\Gamma_{E1} \approx 2$ MeV) has been conventionally used to simulate $E1$ photoabsorption cross sections.

Similar to the present results shown in Fig. 5(b), the previous QRPA calculation for ^{208}Pb that includes only 1p-1h excitation does not reproduce the experimental GDR cross section using a Lorentzian width equal to 0.5 MeV [52]. In contrast, the inclusion of 2 particle, 2 hole (2p-2h) excitation in the shell-model calculation leads to a strong fragmentation of the strength, in particular in the GDR region, and gives a better agreement with the experimental data [52]. Additionally, 1p-1h excitation is dominant below $E = 8$ MeV and 2p-2h effects become important at high energy [52]. This may indicate that a small (large) Lorentzian width is favorable at low (high) energy for theoretical models that consider up to 1p-1h excitation.

Figure 7 shows the $M1$ photoabsorption cross sections (binned in 200 keV steps) for the $J^\pi = 3/2^-$ states deduced from the present $(\vec{\gamma}, \gamma')$ experiment and $(\vec{\gamma}, n)$ experimental data [7]. These data might indicate that two localized $M1$ strengths exist around 6 and 7 MeV, similar to those in ^{206}Pb [17] and ^{208}Pb [6]. In the following, the experimental data are compared with the PVC + QRPA predictions.

In the present calculation, the parameters in the time-odd components of the Skyrme force that influence $M1$ resonances cannot be uniquely determined from the bulk properties of nuclei. Therefore, the same parameter sets of SkM*, SGII, and SkP as used for the $E1$ strength calculation were applied. The calculated $M1$ strengths were folded by the Lorentzian function with $\Gamma_{M1} = 1$ MeV. As shown in Fig. 7, the predicted $M1$ strengths show two peaks for all three Skyrme forces. The lower-energy resonances originate from coherent excitation of $\pi(h^{-1}_{11/2}, h^1_{9/2})$, $\nu(i^{-1}_{13/2}, i^1_{11/2})$, and $\nu(g^{-1}_{9/2}, g^1_{9/2})$ 1p-1h states in the ^{206}Pb core. In particular, the proton $h_{11/2}$ to $h_{9/2}$ transition dominantly contributes to these $M1$ resonances. In contrast, the higher-energy resonances can be attributed to coherent excitation of $\pi(h^{-1}_{11/2}, h^1_{9/2})$ and $\nu(i^{-1}_{13/2}, i^1_{11/2})$ 1p-1h states for the SkM* and SkP forces and $\nu(i^{-1}_{13/2}, i^1_{11/2})$ and $\nu(g^{-1}_{9/2}, g^1_{9/2})$ 1p-1h states for the SGII force.

The energy difference between the peaks predicted by the PVC + QRPA calculations is 2.2 to 2.6 MeV which is approximately twice that deduced from the experimental data if taking $E = 7.24$ MeV for the higher-energy peak. As mentioned above, the present PVC + QRPA calculations include only 1p-1h excitation. The coupling to 2p-2h states leads to fragmentation of the $M1$ strength [53,54]. In addition, the tensor force is important for describing the $M1$ strength distribution [53,55]. The inclusion of such residual interactions in the present PVC + QRPA model is a challenge for the future.

V. SUMMARY

In summary, NRF experiments on ^{207}Pb have been performed using a quasimonochromatic, linearly polarized photon beam. From the present measurement, the spins and/or

parities of the states observed in ^{207}Pb were determined. The present results, combined with previous (γ, n) data, were used to investigate the $E1$ and $M1$ photoabsorption cross sections by comparison with predictions from the particle-vibration coupling (PVC) with the quasiparticle random-phase approximation (QRPA) model. The PVC + QRPA calculations reproduce the gross properties of the dipole strengths observed near the neutron separation energy. While the coupling of a neutron with the low-lying 3^- states of the ^{206}Pb core is important for the $E1$ strength at low energy, higher-order mixing than 1p-1h is required for describing the strength distribution at higher energy in the GDR region. In addition, the present calculations suggest that the coherent excitations of spin-flip 1p-1h states in the ^{206}Pb core is responsible for the $M1$ strength near the neutron separation energy.

ACKNOWLEDGMENTS

This work was supported in part by Grants-in-Aid for Scientific Research (C) (17K05482, 18H03715, and 20K04007) from the Japan Society for the Promotion of Science (JSPS).

[1] K. Heyde, P. von Neumann-Cosel, and A. Richter, Rev. Mod. Phys. **82**, 2365 (2010).
[2] D. Savran, T. Aumann, and A. Zilges, Prog. Part. Nucl. Phys. **70**, 210 (2013).
[3] M. N. Harakeh and A. van der Woude, *Giant Resonances: Fundamental High-Frequency Modes of Nuclear Excitation* (Clarendon Press, Oxford, 2001).
[4] R. M. Laszewski, R. Alarcon, D. S. Dale, and S. D. Hoblit, Phys. Rev. Lett. **61**, 1710 (1988).
[5] R. Köhler, J. A. Wartena, H. Weigmann, L. Mewissen, F. Poortmans, J. P. Theobald, and S. Raman, Phys. Rev. C **35**, 1646 (1987).
[6] T. Shizuma, T. Hayakawa, H. Ohgaki, H. Toyokawa, T. Komatsubara, N. Kikuzawa, A. Tamii, and H. Nakada, Phys. Rev. C **78**, 061303(R) (2008).
[7] T. Kondo, H. Utsunomiya, S. Goriely, I. Daoutidis, C. Iwamoto, H. Akimune, A. Okamoto, T. Yamagata, M. Kamata, O. Itoh, H. Toyokawa, Y.-W. Lui, H. Harada, F. Kitatani, S. Hilaire, and A. J. Koning, Phys. Rev. C **86**, 014316 (2012).
[8] A. Leistenschneider *et al.*, Phys. Rev. Lett. **86**, 5442 (2001).
[9] N. Ryezayeva, T. Hartmann, Y. Kalmykov, H. Lenske, P. von Neumann-Cosel, V. Yu. Ponomarev *et al.*, Phys. Rev. Lett. **89**, 272502 (2002).
[10] T. Hartmann, M. Babilon, S. Kamerdzhiev, E. Litvinova, D. Savran, S. Volz, and A. Zilges, Phys. Rev. Lett. **93**, 192501 (2004).
[11] P. Adrich, A. Klimkiewicz, M. Fallot, K. Boretzky, T. Aumann, D. Cortina-Gil *et al.*, Phys. Rev. Lett. **95**, 132501 (2005).
[12] O. Wieland *et al.*, Phys. Rev. Lett. **102**, 092502 (2009).
[13] D. Savran, M. Fritzsche, J. Hasper, K. Lindenberg, S. Müller, V. Yu. Ponomarev, K. Sonnabend, and A. Zilges, Phys. Rev. Lett. **100**, 232501 (2008).
[14] R. Schwengner, G. Rusev, N. Tsoneva, N. Benouaret, R. Beyer, M. Erhard, E. Grosse, A. R. Junghans, J. Klug, K. Kosev, H. Lenske, C. Nair, K. D. Schilling, and A. Wagner, Phys. Rev. C **78**, 064314 (2008).
[15] A. P. Tonchev, S. L. Hammond, J. H. Kelley, E. Kwan, H. Lenske, G. Rusev, W. Tornow, and N. Tsoneva, Phys. Rev. Lett. **104**, 072501 (2010).
[16] R. Schwengner, R. Massarczyk, G. Rusev, N. Tsoneva, D. Bemmerer, R. Beyer, R. Hannaske, A. R. Junghans, J. H. Kelley, E. Kwan, H. Lenske, M. Marta, R. Raut, K. D. Schilling, A. Tonchev, W. Tornow, and A. Wagner, Phys. Rev. C **87**, 024306 (2013).
[17] A. P. Tonchev, N. Tsoneva, C. Bhatia, C. W. Arnold, S. Goriely, S. L. Hammond, J. H. Kelley, E. Kwan, H. Lenske, J. Piekarewicz, R. Raut, G. Rusev, T. Shizuma, and W. Tornow, Phys. Lett. B **773**, 20 (2017).
[18] J. Piekarewicz, Phys. Rev. C **73**, 044325 (2006).
[19] A. Brown, Phys. Rev. Lett. **85**, 5296 (2000).
[20] J. Enders, P. von Brentano, J. Eberth, A. Fitzler, C. Fransen, R.-D. Herzberg, H. Kaiser, L. Käubler, P. von Neumann-Cosel, N. Pietralla, V. Yu. Ponomarev, H. Prade, A. Richter, H. Schnare, R. Schwengner, S. Skoda, H. G. Thomas, H. Tiesler, and I. Wiedenhöver, Phys. Lett. B **486**, 279 (2000).
[21] C. P. Swann, J. Franklin Inst. **298**, 321 (1974).
[22] D. F. Coope, L. E. Cannell, and M. K. Brussel, Phys. Rev. C **15**, 1977 (1977).
[23] T. Chapuran, R. Vodhanel, and M. K. Brussel, Phys. Rev. C **22**, 1420 (1980).
[24] A. Nord, S. W. Yates, O. Beck, D. Belic, P. von Brentano, T. Eckert, C. Fransen, R.-D. Herzberg, U. Kneissl, H. Maser, N. Pietralla, H. H. Pitz, and V. Werner, Phys. Rev. C **57**, 3459 (1998).
[25] J. Enders, P. von Brentano, J. Eberth, A. Fitzler, C. Fransen, R.-D. Herzberg, H. Kaiser, L. Käubler, P. von Neumann-Cosel, N. Pietralla, V. Yu. Ponomarev, A. Richter, R. Schwengner, and I. Wiedenhöver, Nucl. Phys. A **724**, 243 (2003).
[26] N. Pietralla, T. C. Li, M. Fritzsche, M. W. Ahmed, T. Ahn, A. Costin, J. Enders, J. Li, S. Müller, P. von Neumann-Cosel, I. V. Pinayev, V. Yu. Ponomarev, D. Savran, A. P. Tonchev, W. Tornow, H. R. Weller, V. Werner, Y. K. Wu, and A. Zilges, Phys. Lett. B **681**, 134 (2009).
[27] A. Bohr and B. R. Motteleson, *Nuclear Structure Vol. II: Nuclear Deformations* (World Scientific Publishing Co. Pte. Ltd, 1998).
[28] P. Ring and P. Schuck, *The Nuclear Many-Body Problem* (Springer-Verlag, Berlin, 1980).
[29] S. Miyamoto, Y. Asano, S. Amano, D. Li, K. Imasaki, H. Kinugasa, Y. Shoji, T. Takagi, and T. Mochizuki, Radiat. Meas. **41**, S179 (2006).
[30] S. Amano, K. Horikawa, K. Ishihara, S. Miyamoto, T. Hayakawa, T. Shizuma, and T. Mochizuki, Nucl. Instrum. Methods Phys. Res., Sect. A **602**, 337 (2009).
[31] H. Hirayama, Y. Namito, A. F. Bielajew, S. J. Wilderman, and W. R. Nelson, The EGS5 Code System, SLAC-R-730 (2005) and KEK Report 2005-8 (2005).
[32] L. W. Fagg and S. S. Hanna, Rev. Mod. Phys. **31**, 711 (1959).
[33] U. Kneissl, H. H. Pitz, and A. Zilges, Prog. Part. Nucl. Phys. **37**, 349 (1996).

[34] F. Metzger, in *Progress in Nuclear Physics*, edited by O. Frisch (Pergamon Press, New York, 1959), Vol. 7, pp. 53–88.
[35] F. G. Kondev and S. Lalkovski, Nucl. Data Sheets **112**, 707 (2011).
[36] W. T. Wagner, G. M. Crawley, and G. R. Hammerstein, Phys. Rev. C **11**, 486 (1975).
[37] E. Lipparini and A. Richter, Phys. Lett. B **144**, 13 (1984).
[38] R. R. Harvey, J. T. Caldwell, R. L. Bramblett, and S. C. Fultz, Phys. Rev. **136**, B126 (1964).
[39] B. L. Berman, R. E. Pywell, S. S. Dietrich, M. N. Thompson, K. G. McNeill, and J. W. Jury, Phys. Rev. C **36**, 1286 (1987).
[40] J. Kopecky and M. Uhl, Phys. Rev. C **41**, 1941 (1990).
[41] J. Enders, M. Babilon, T. Hartmann, A. Heine, P. von Neumann-Cosel, V. Yu. Ponomarev, N. Ryezayeva, S. Volz, A. Zilges, and T. Guhr, Acta Phys. Pol., B **36**, 1077 (2005).
[42] R. Capote, M. Herman, P. Obložinský, P. G. Young, S. Goriely, T. Belgya, A. V. Ignatyuk, A. J. Koning, S. Hilaire, V. A. Plujko, M. Avrigeanu, O. Bersillon, M. B. Chadwick, T. Fukahori, Z. Ge, Y. Han, S. Kailas, J. Kopecky, and P. Talouc, Nucl. Data Sheets **110**, 3107 (2009).
[43] D. Vautherin and D. M. Brink, Phys. Rev. C **5**, 626 (1972).
[44] D. Vautherin, Phys. Rev. C **7**, 296 (1973).
[45] J. Dobaczewski and J. Dudek, Phys. Rev. C **52**, 1827 (1995).
[46] K. Yoshida, Phys. Rev. C **79**, 054303 (2009).
[47] F. Minato and Y. Tanimura, Eur. Phys. J. A **56**, 45 (2020).
[48] J. Bartel, P. Quentin, M. Brack, C. Guet, and H.-B. Hakansson, Nucl. Phys. A **386**, 79 (1982).
[49] Van Giai Nguyen and H. Sagawa, Phys. Lett. B **106**, 379 (1981).
[50] J. Dobaczewski, H. Flocard, and J. Treiner, Nucl. Phys. A **422**, 103 (1984).
[51] I. Hamamoto, Nucl. Phys. A **126**, 545 (1969).
[52] R. Schwengner, R. Massarczyk, B. A. Brown, R. Beyer, F. Dönau, M. Erhard, E. Grosse, A. R. Junghans, K. Kosev, C. Nair, G. Rusev, K. D. Schilling, and A. Wagner, Phys. Rev. C **81**, 054315 (2010).
[53] J. Speth, V. Klemt, J. Wambach, and G. E. Brown, Nucl. Phys. A **343**, 382 (1980).
[54] D. Cha, B. Schwesinger, J. Wambach, and J. Speth, Nucl. Phys. A **430**, 321 (1984).
[55] J. Wambach, A. D. Jackson, and J. Speth, Nucl. Phys. A **348**, 221 (1980).